Demonstration of AlGaN/GaN-based ultraviolet phototransistor with a record high responsivity over 3.6×10^7 A/W

Cite as: Appl. Phys. Lett. **118**, 242105 (2021); doi: 10.1063/5.0055468
Submitted: 29 April 2021 · Accepted: 31 May 2021 ·
Published Online: 17 June 2021

View Online Export Citation CrossMark

Haochen Zhang, Fangzhou Liang, Kang Song, Chong Xing, Danhao Wang, Huabin Yu, Chen Huang, Yue Sun, Lei Yang, Xiaolong Zhao, Haiding Sun,[a] and Shibing Long

AFFILIATIONS

School of Microelectronics, University of Science and Technology of China, Hefei, Anhui 230026, China

[a]Author to whom correspondence should be addressed: haiding@ustc.edu.cn

ABSTRACT

In this work, we demonstrate a high-performance ultraviolet phototransistor (UVPT) based on the AlGaN/GaN high-electron mobility transistor (HEMT) configuration. When the device is biased at off state, the peak photoresponsivity (R) of 3.6×10^7 A/W under 265 nm illumination and 1.0×10^6 A/W under 365 nm illumination can be obtained. Those two R values are one of the highest among the reported UVPTs at the same detection wavelength under off-state conditions. In addition, we investigate the gate-bias (V_{GS}) dependent photoresponse of the fabricated device with the assistance of band structure analysis. It was found that a more negative V_{GS} can significantly reduce the rise/decay time for 265 nm detection, especially under weak illumination. This can be attributed to a largely enhanced electric field in the absorptive AlGaN barrier that pushes the photo-generated carriers rapidly into the GaN channel. In contrast, the V_{GS} has little impact on the switching time for 365 nm photodetection, since the GaN channel has a larger absorption depth and the entire UVPT simply acts as a photoconductive-type device. In short, the proposed AlGaN/GaN HEMT structure with the superior photodetection performance paves the way for the development of next generation UVPTs.

The pursuit of the high-efficient ultraviolet photodetectors (UV PDs) has lasted for decades to meet the requirements in both civil and military applications such as fire alarm, space exploration, missile detection, and secure communication.[1–3] Among multiple materials that have been employed for UV detection, III-nitride semiconductors, typified by GaN alloys, stand out as one of the top contenders thanks to their wide bandgap, large UV absorption coefficient, excellent chemical stability, and high carrier mobility.[4,5] Therefore, various device structures of GaN-based UV PDs, such as photoelectrochemical (PEC),[6–8] p-i-n,[9] Schottky,[10] and metal-semiconductor-metal (MSM),[11] have been proposed and intensively studied. In addition to those conventional configurations, an AlGaN(InAlN)/GaN hetero-junction, which is the key building block for high-electron mobility transistors (HEMTs), has recently gained much attention to build UV PDs.[12–20] Due to the inherent polarization effects of III-nitride materials, there exist high-concentration and high-mobility two dimensional electron gases (2DEGs) at the AlGaN/GaN hetero-interface.[4] As a result, such UV PDs usually possess large photocurrent (I_{photo}), high photoresponsivity (R), and transistor-like electrical and optical performance, which have great potential in UV imaging and optical communication.[1,21]

However, the spontaneously formed 2DEG would lead to inferior noise performance, namely, high dark current (I_{dark}) and low detectivity (D^*) during device operation. For instance, an AlGaN/GaN UV PD could possibly produce a high R exceeding 10^9 A/W, whereas its I_{dark} had the same order of magnitude as I_{photo} (∼mA).[22] Therefore, such devices can hardly be utilized for accurate and reliable UV detection. To suppress dark current, an additional gate control should be employed to deplete the 2DEG channel under dark conditions, making the AlGaN/GaN UV PDs operate at the off state. In this regard, p-GaN cap layers,[12,13] recessed AlGaN barrier layer,[14,15] and semi-transparent gate contacts[16–20] have been tentatively adopted in the device fabrication process. Among those device architectures, a negatively biased semi-transparent gate is a straightforward configuration requiring simplest fabrication process, in addition to the avoidance of the UV absorptive p-GaN layers as well as the etching damage in those recessed AlGaN layers. To realize the off-state operation, the metal-gated AlGaN/GaN ultraviolet phototransistor (UVPT) should be biased under V_{GS} (gate voltage) $< V_{th}$ (threshold voltage) conditions.

In this work, we demonstrate a UVPT based on AlGaN/GaN HEMT configuration using a 10/10 nm Ni/Au semitransparent gate. When the device is biased at off state, a low dark current of 20 pA can be achieved. More importantly, a superior photodetection behavior can be obtained, featuring the peak R values of 3.6×10^7 A/W under 265 nm UV illumination and 1.0×10^6 A/W under 365 nm UV illumination, respectively. A further study in the V_{GS}-dependent photoresponse of the UVPT reveals that a more negative V_{GS} would significantly reduce the rise/decay time for 265 nm detection thanks to an increased electric field in the absorptive AlGaN barrier layer. In contrast, the V_{GS} has little impact on the switching process for 365 nm detection, since the GaN channel has a larger absorption depth and the device operates in the photoconductive mode. In end, the underlying mechanism was analyzed with detailed energy band diagram investigations.

The investigated sample in this study was grown on a sapphire substrate by metal-organic chemical vapor deposition (MOCVD).[23] The epitaxial structure consists of an AlN nucleation layer, a 5 μm GaN buffer layer, a 1.7 μm unintentionally doped (UID) GaN layer, a 1 nm AlN spacer layer, a 50 nm $Al_{0.3}Ga_{0.7}N$ barrier layer, and a 3 nm GaN cap layer. The dislocation density of the epitaxial structure was measured as 6.9×10^8 cm^{-2} by XRD measurement. The as-received wafer was cleaned in acetone/isopropanol/de-ionized water in sequence before device fabrication. Then Cl_2-based inductively coupled plasma (ICP) etching was employed for mesa formation and device isolation. Ti/Al/Ni/Au metal stacks were employed as the source/drain Ohmic contacts followed by a N_2 rapid thermal process. Finally, a 10/10 nm Ni/Au semitransparent gate was e-beam evaporated to form a Schottky gate contact. Figure 1(a) schematically shows the device structure of the AlGaN/GaN UVPT. The UV transmission of the gate contact is measured as 14.81% for 265 nm and 21.42% for 365 nm, as shown in Fig. 1(b). The nominal gate length (L_G) and gate width (W_G) of the fabricated device were 2 and 10 μm, respectively, giving a UV absorption area of 20 μm^2. To investigate the optical properties of the fabricated UVPT, we employed 265 and 365 nm UV LEDs as the light sources. The light intensity was calibrated by an optical power meter (2936-R, Newport). The electrical performance of the UVPT was tested by a semiconductor device analyzer (B1500A, Keysight).

The measured transfer characteristics of the UVPT under different light sources are plotted in Figs. 2(a) and 2(b). As discussed previously, the UVPT should be operated at the off state. Therefore, we

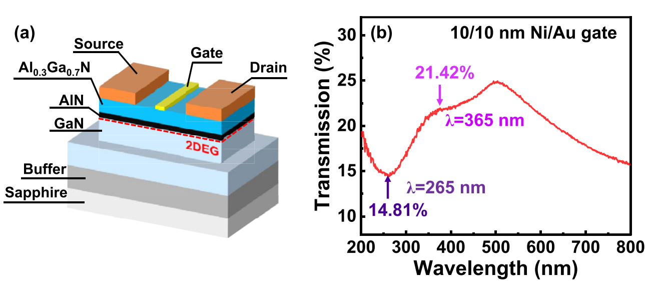

FIG. 1. (a) Schematic of the fabricated AlGaN/GaN UVPT. (b) UV transmission of the 10/10 nm Ni/Au gate metal.

mainly focus on the electrical and optical properties under $V_{GS} < V_{th}$ conditions. Under dark conditions, the device exhibits a low I_{dark} on the order of ~pA at the cutoff region and an ON/OFF ratio of 2.5×10^8 at a drain voltage (V_{DS}) of 8 V, which lays the basic foundation of a high-performance UVPT. When the device was under external UV illumination, excess photo-generated carries were produced, leading to the negatively shifted V_{th} as the light intensity increases. Furthermore, the R and photo-to-dark-current ratio ($PDCR$) values of the UVPT under 265 and 365 nm illumination are extracted from the transfer curves at $V_{GS} = -8.2$ V, where I_{dark} reaches the lowest value of 20 pA. Meanwhile, the corresponding external quantum efficiency (EQE) and detectivity ($D*$) can also be calculated. The expressions of those critical parameters are given by: $PDCR = (I_{photo} - I_{dark})/I_{dark}$, $R = (I_{photo} - I_{dark})/PS$ (P is the light power intensity and S is the UV absorption area), $EQE = hcR/q\lambda$ (h, c, q, and λ are Plank's constant, velocity of light, elementary electric charge, and light wavelength, respectively), and $D^* = RS^{1/2}/(2qI_{dark})^{1/2}$.[24]

The maximum $PDCR$ are obtained at the highest UV light intensity, i.e., 8.1×10^7 for 265 nm at 3.75 mW/cm^2 and 3.6×10^7 for 365 nm at 7.00 mW/cm^2. The peak R values are calculated as 3.6×10^7 (265 nm, 12 μW/cm^2) and 1.0×10^6 (365 nm, 340 μW/cm^2), respectively. The corresponding maximum EQE and $D*$ for 265/365 nm detection are 1.7×10^8%/3.4×10^6% and 6.5×10^{18}/1.8×10^{17} Jones, respectively. Table I benchmarks the performance of the UVPT along with the reported state-of-the-art UVPTs based on wide bandgap Al(Ga)N and Ga_2O_3 materials. The bias conditions of these devices are included, and all the results are extracted under off-state conditions, namely, $V_{GS} < V_{th}$. It can be found that our Ni/Au-gated AlGaN/GaN UVPT possesses the record-high R and EQE for both 365 nm[13–15,20] and solar-blind detection.[17,25–27] We believe the performance of our AlGaN/GaN UVPTs can be further improved via optimizing ICP etching, post-etch treatment, and gate metal deposition schemes.

It should be noted that R reaches the first peak value of 6.9×10^5 under 365 nm UV light at 21.8 μW/cm^2, as shown in Fig. 2(d). This is possibly because the photo-induced carriers can only exist in the depleted channel at the AlGaN/GaN hetero-interface under weak light detection. When the UV intensity increases, the excess carriers are generated in the beneath GaN channel and a second R peak occurs under strong light illumination of 340 μW/cm^2.

To further evaluate the switching behavior of the fabricated UVPT, we performed the characterizations of the photoresponse time of the device under 265 and 365 nm UV illumination with various light intensities. The device was biased under a constant $V_{DS} = 8$ V. Then, we characterized the device by operating it under two representing applied gate biases, i.e., $V_{GS} = -8.2$ V (close to V_{th}) and a more negative $V_{GS} = -12$ V. The V_{GS}-dependent photoresponse of the fabricated UVPT is plotted in Figs. 3(a)–3(d). The insets present the enlarged switching process under different UV intensities for a clear comparison. It can be found that under relatively weak 265 nm-light conditions (light intensity < 830 μW/cm^2), the rise time (t_r, defined as the time of the photocurrent increases from 10% to 90%) and decay time (t_d, defined as the time of the photocurrent decreases from 90% to 10%) of our UVPT under $V_{GS} = -12$ V are reduced by two orders of magnitude compared with that under $V_{GS} = -8.2$ V, as shown in Fig. 3(e). We suspect that, with a more negative V_{GS}, the electric field within the AlGaN barrier layer would be largely enhanced, leading to

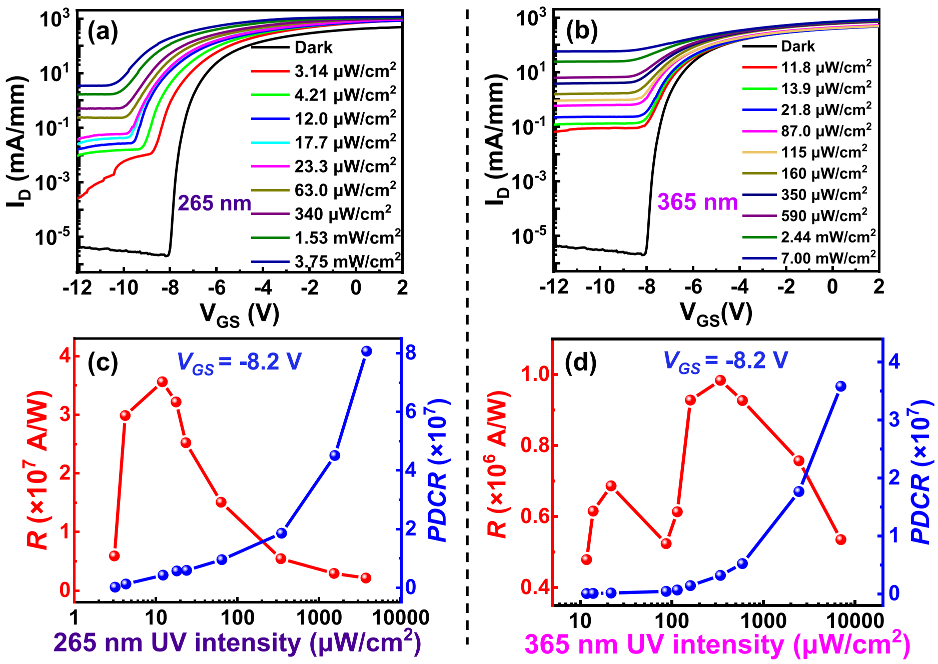

FIG. 2. The transfer curves of the UVPT under (a) 265 nm and (b) 365 nm UV illumination with various incident power. (c) and (d) show the extracted and *R* and *PDCR* under different UV intensities.

an increase in the barrier height ($\Phi_{265\,nm}$) by ~1.4 eV when V_{GS} changes from −8.2 V to −12 V, as illustrated in Figs. 4(a) and 4(b). Moreover, such weak light illumination can only excite a relatively small number of photo-generated carriers. Consequently, these photo-generated carriers can be driven from the barrier to the channel in a faster speed, so that the photoresponse time is greatly shortened. Interestingly, when the intensity of 265 nm light increases to 3.75 mW/cm^2, the photoresponse time of our device under V_{GS} of −8.2 and −12 V are very close to each other, within the range of 20–100 ms, which can be attributed to the fact that the entire AlGaN barrier was excited by strong illumination to generate sufficient photo-induced carriers, which filled up the entire barrier. Additionally, under such strong light illumination, the incident 265 nm light could also reach the bottom GaN bulk and get absorbed by the GaN layer. In this case, the change of V_{GS} has little impact on the transport process and thus the response time of the device. This phenomenon is consistent with the observation in Fig. 3(f), where the photoresponse time of the device under 365 nm illumination remains almost the same under V_{GS} of −12 and −8.2 V, since 365 nm photons can only be absorbed by the GaN bulk and the response behavior is independent to the V_{GS}.

Furthermore, the distinct difference between t_r and t_d of the device under 265 and 365 nm light illumination can be observed, as shown in Fig. 3. Such difference is highly related to the device operating principle of our AlGaN/GaN-based UVPT structure. On one hand, 365 nm light can only excite the GaN bulk layer no matter how weak or strong the light intensity was. In contrast, under 265 nm light illumination, both GaN and AlGaN layers can respond to the incident light. In one scenario, under weak light illumination, most of the light is absorbed by the AlGaN barrier. In another scenario, both GaN bulk and AlGaN barriers may absorb the 265 nm light once the light

TABLE I. Comparison of the optical performance (*R*, *EQE*, *D**) of the UVPTs based on GaN and Ga_2O_3 materials reported recently. The bias conditions (V_{GS}/V_{DS}) for device operation are included. *R* represents responsivity. *EQE* represents external quantum efficiency. *D** represents detectivity. V_{GS}/V_{DS} represents biased gate/drain voltage.

Structure	λ (nm)	Bias conditions (V)	R (A/W)	EQE (%)	D∗ (Jones)
$Al_{0.45}Ga_{0.55}N/Al_{0.3}Ga_{0.7}N$ UVPT (Ref. 17)	280	$V_{GS}/V_{DS} = -2/5$	6.2×10^4	2.7×10^5	—
Quasi-2D Ga_2O_3 UVPT (Ref. 25)	254	$V_{GS}/V_{DS} = -20/20$	4.8×10^5	2.3×10^6	6.7×10^{14}
β-Ga_2O_3 Microflake phototransistor (Ref. 26)	254	$V_{GS}/V_{DS} = -10/6$	1.7×10^5	8.4×10^5	1.2×10^{18}
β-Ga_2O_3 MOS phototransistor (Ref. 27)	254	$V_{GS}/V_{DS} = -27/15$	1.4×10^7	6.4×10^7	1.1×10^{19}
This work	**265**	$\mathbf{V_{GS}/V_{DS} = -8.2/8}$	$\mathbf{3.6 \times 10^7}$	$\mathbf{1.7 \times 10^8}$	$\mathbf{6.5 \times 10^{18}}$
AlGaN/GaN with recessed barrier (Ref. 16)	312	$V_{GS}/V_{DS} = 0/100$	7×10^4	2.8×10^5	—
ITO/AlGaN/GaN UVPT (Ref. 20)	360	$V_{GS}/V_{DS} = -3.1/6$	2×10^5	6.8×10^5	—
p-GaN/AlGaN/GaN photodetector (Ref. 14)	365	$V_{GS}/V_{DS} = 0/5$	6×10^5	2.0×10^6	—
p-GaN/AlGaN/GaN photodetector (Ref. 13)	365	$V_{GS}/V_{DS} = 0/5$	2×10^4	6.8×10^4	1.4×10^{14}
This work	**365**	$\mathbf{V_{GS}/V_{DS} = -8.2/8}$	$\mathbf{1.0 \times 10^6}$	$\mathbf{3.4 \times 10^6}$	$\mathbf{1.8 \times 10^{17}}$

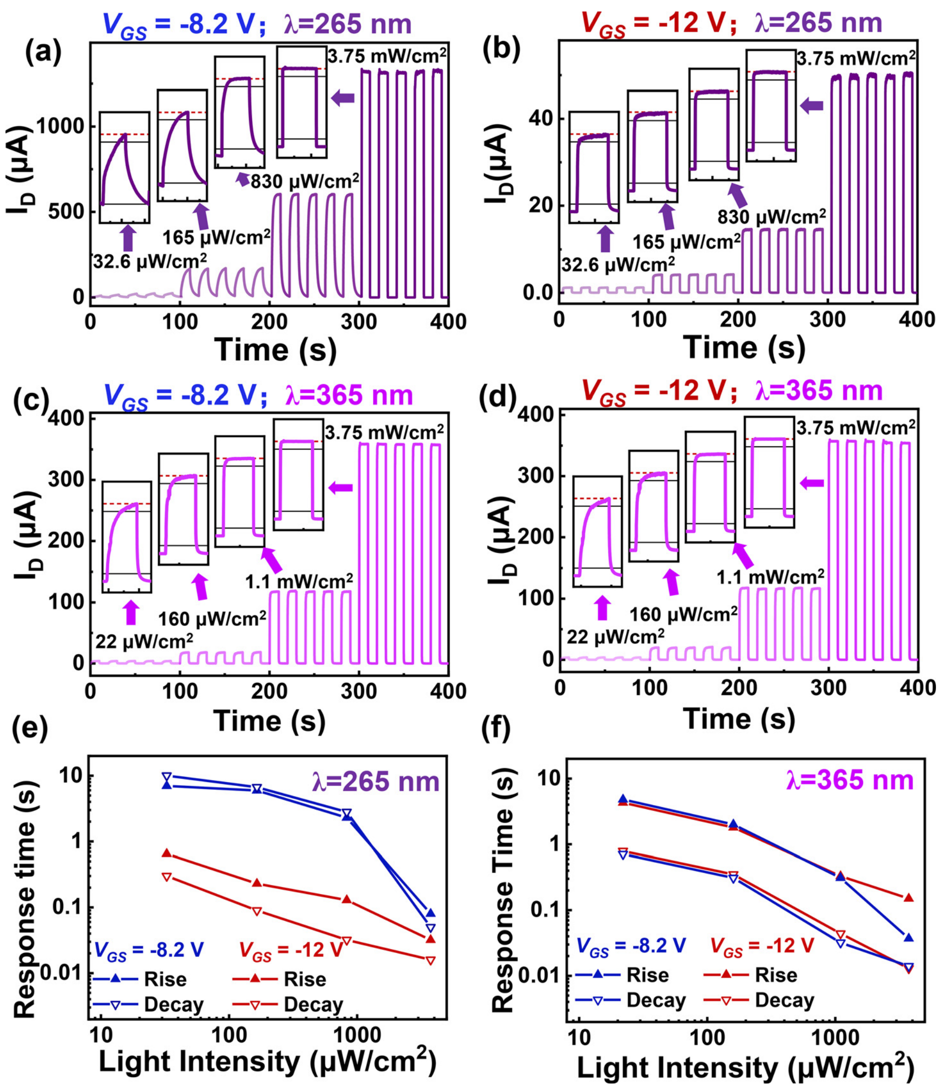

FIG. 3. The photoresponse of the UVPT under: (a) 265 nm UV light, $V_{GS} = -8.2$ V, (b) 265 nm UV light, $V_{GS} = -12$ V, (c) 365 nm UV light, $V_{GS} = -8.2$ V, and (d) 365 nm UV light, $V_{GS} = -12$ V. The insets are the enlarged switching process under various UV intensities. The extracted t_r/t_d under 265 and 365 nm illumination are plotted in (e) and (f), respectively.

intensity was strong enough to penetrate through the entire AlGaN barrier and reach to the bottom GaN bulk. Therefore, the difference of the photoresponse time under 265 and 365 nm light should be attributed to the different absorption mechanism in our device, not to mention that the photoresponse time is also strongly affected by the applied V_{GS} and the corresponding band structures, as we have explained in detail how the applied V_{GS} affects the photoresponse time under 265 nm previously.

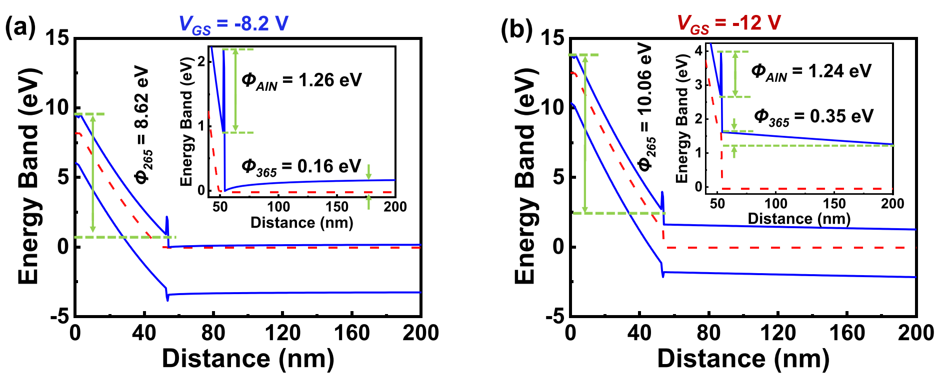

FIG. 4. Calculated band diagrams of the AlGaN/GaN UVPT under (a) $V_{GS} = -8.2$ V and (b) -12 V, respectively.

Moreover, a significant drop of t_r/t_d with increased light intensity for both 265 and 365 nm illumination can be observed, as displayed in Figs. 3(e) and 3(f). Under a weak light condition, the slow photoresponse of UVPT can be attributed to a low generation rate of photo-induced carriers in both the AlGaN barrier (265 nm absorption) and GaN channel (365 nm absorption). In addition, the AlN spacer layer can form a 1.26 and 1.24 eV barrier height at the AlGaN/GaN heterointerface under V_{GS} of −8.2 and −12 V, as shown in the inset of Figs. 4(a) and 4(b), which may further block the photo-generated carriers from migration into the channels. However, when the UV intensity continuously increases, the generation rate would be enhanced drastically, leading to a relatively fast response under 265 and 365 nm illumination. It should be noted that the photoresponse process of our AlGaN/GaN-based UVPT is still relatively slow since massive carriers should be photogenerated and diminished during the light ON/OFF switching process considering the ultra-high *PDCR* and *R* values of the devices. Furthermore, the persistent photocurrent (PPC) effect, which has been widely reported in the GaN-based UV PDs, would also contribute to the large response time.[16] A typical resulted non-exponential decay process can also be observed in our fabricated UVPT.

In summary, we have demonstrated a semi-transparent Ni/Au-gated AlGaN/GaN UVPT with high *R* for both 265 (3.6×10^7 A/W at 12 μW/cm^2) and 365 nm (1.0×10^6 A/W at 340 μW/cm^2) photodetection at the off state. A low I_{dark} of 20 pA, remarkable *PDCR*, and ultra-high D$*$ ($6.5 \times 10^{18}/1.8 \times 10^{17}$ Jones for 265/365 nm detection) are also obtained. Importantly, an investigation into the V_{GS}-dependent photoresponse of the UVPT with the assistance of a band structure analysis was performed, revealing that a negative V_{GS} can increase the electric field of the AlGaN barrier and therefore significantly shorten the t_r/t_d of UVPT for 265 nm UV detection, especially under weak light conditions. In contrast, V_{GS} has little impact on t_r/t_d for 365 nm illumination, because the GaN channel has a deep absorption depth, and the device mainly works in the photoconductive mode. In short, the superior photodetection behavior of our AlGaN/GaN UVPT provides a feasible device architecture to promote the development of high-performance UV PDs based on wide bandgap semiconductors of the future.

This work was funded by the National Natural Science Foundation of China (Grant Nos. 61905236 and 51961145110), the Fundamental Research Funds for the Central Universities (Grant No. WK2100230020), USTC Research Funds of the Double First-Class Initiative (Grant No. YD3480002002), and was partially carried out at the USTC Center for Micro and Nanoscale Research and Fabrication.

DATA AVAILABILITY

The data that support the findings of this study are available from the corresponding author upon reasonable request.

REFERENCES

[1] C. Huang, H. Zhang, and H. Sun, Nano Energy **77**, 105149 (2020).
[2] Q. Cai, H. You, H. Guo, J. Wang, B. Liu, Z. Xie, D. Chen, H. Lu, Y. Zheng, and R. Zhang, Light Sci. Appl. **10**, 94 (2021).
[3] X. Hou, Y. Zou, M. Ding, Y. Qin, Z. Zhang, X. Ma, P. Tan, S. Yu, X. Zhou, X. Zhao, G. Xu, H. Sun, and S. Long, J. Phys. D: Appl. Phys. **54**, 043001 (2021).
[4] H. Zhang, C. Huang, K. Song, H. Yu, C. Xing, D. Wang, Z. Liu, and H. Sun, Rep. Prog. Phys. **84**, 044401 (2021).
[5] J. Chen, W. Ouyang, W. Yang, J. H. He, and X. Fang, Adv. Funct. Mater. **30**, 1909909 (2020).
[6] S. Fang, D. Wang, X. Wang, X. Liu, Y. Kang, H. Yu, H. Zhang, W. Hu, J. He, H. Sun, and S. Long, "Tuning the charge transfer dynamics of the nanostructured GaN photoelectrodes for efficient photoelectrochemical detection in the ultraviolet band," Adv. Funct. Mater. (published online, 2021).
[7] D. Wang, X. Liu, S. Fang, C. Huang, Y. Kang, H. Yu, Z. Liu, H. Zhang, R. Long, Y. Xiong, Y. Lin, Y. Yue, B. Ge, T. Ng, B. Ooi, Z. Mi, J. He, and H. Sun, Nano Lett. **21**, 120 (2021).
[8] D. Wang, C. Huang, X. Liu, H. Zhang, H. Yu, S. Fang, B. S. Ooi, Z. Mi, J. H. He, and H. Sun, Adv. Opt. Mater. **9**, 2000893 (2021).
[9] W. Xu, Y. Shi, F. Ren, D. Zhou, L. Su, Q. Liu, L. Cheng, J. Ye, D. Chen, R. Zhang, Y. Zheng, and H. Lu, Photonics Res. **7**, B48 (2019).
[10] F. Liang, M. Feng, Y. Huang, X. Sun, X. Zhan, J. Liu, Q. Sun, R. Wang, X. Ge, J. Ning, and H. Yang, Opt. Express **28**, 17188 (2020).
[11] S. Chang, M. Chang, and Y. Yang, IEEE Photonics J. **9**, 6801707 (2017).
[12] B. Pandit and E. F. Schubert, J. Cho, Sci. Rep. **10**, 22059 (2020).
[13] Q. Lyu, H. Jiang, and K. M. Lau, Appl. Phys. Lett. **117**, 071101 (2020).
[14] M. Ishiguro, K. Ikeda, M. Mizuno, M. Iwaya, T. Takeuchi, S. Kamiyama, and I. Akasaki, Jpn. J. Appl. Phys. **52**, 08jf02 (2013).
[15] P. Satterthwaite, A. Yalamarthy, N. Scandrette, A. K. M. Newaz, and D. Senesky, ACS Photonics **5**, 4277 (2018).
[16] M. Martens, J. Schlegel, P. Vogt, F. Brunner, R. Lossy, J. Würfl, M. Weyers, and M. Kneissl, Appl. Phys. Lett. **98**, 211114 (2011).
[17] A. Armstrong, B. Klein, A. Allerman, E. Douglas, A. Baca, M. Crawford, G. Pickrell, and C. Sanchez, J. Appl. Phys. **123**, 114502 (2018).
[18] S. Kumar, A. Pratiyush, S. Dolmanan, S. Tripathy, R. Muralidharan, and D. Nath, Appl. Phys. Lett. **111**, 251103 (2017).
[19] L. Li, D. Hosomi, Y. Miyachi, T. Hamada, M. Miyoshi, and T. Egawa, Appl. Phys. Lett. **111**, 102106 (2017).
[20] T. Narita, A. Wakejima, and T. Egawa, Jpn. J. Appl. Phys. **52**, 01AG06 (2013).
[21] Q. Lyu, H. Jiang, and K. Lau, Opt. Express **29**, 8358 (2021).
[22] T. Kuan, S. Chang, Y. Su, C. Ko, J. Webb, J. Bardwell, Y. Liu, H. Tang, W. Lin, Y. Cherng, and W. Lan, Jpn. J. Appl. Phys. **42**, 5563 (2003).
[23] H. Sun, S. Mitra, R. Subedi, Y. Zhang, W. Guo, J. Ye, M. Shakfa, T. Ng, B. Ooi, I. Roqan, Z. Zhang, J. Dai, C. Chen, and S. Long, Adv. Funct. Mater. **48**, 1905445 (2019).
[24] W. Kong, G. Wu, K. Wang, T. Zhang, Y. Zou, D. Wang, and L. Luo, Adv. Mater. **28**, 10725 (2016).
[25] Y. Liu, L. Du, G. Liang, W. Mu, Z. Jia, M. Xu, Q. Xin, X. Tao, and A. Song, IEEE Electron Device Lett. **39**, 1696 (2018).
[26] S. Yu, X. Zhao, M. Ding, P. Tan, X. Hou, Z. Zhang, W. Mu, Z. Jia, X. Tao, G. Xu, and S. Long, IEEE Electron Device Lett. **42**, 383 (2021).
[27] Z. Li, Z. Feng, Y. Xu, Q. Feng, W. Zhu, D. Chen, H. Zhou, J. Zhang, C. Zhang, and Y. Hao, IEEE Electron Device Lett. **42**, 545 (2021).